JTTEE5 17:762–773
DOI: 10.1007/s11666-008-9252-7
1059-9630/$19.00 © ASM International

Erosion, Abrasive, and Friction Wear Behavior of Iron Aluminide Coatings Sprayed by HVOF

J.M. Guilemany, N. Cinca, J. Fernández, and S. Sampath

(Submitted May 3, 2008; in revised form September 22, 2008)

Iron aluminides have been proposed lately as promising materials for wear applications. Many authors have focused their investigations on the friction behavior of FeAl coatings, emphasizing the role of this intermetallic phase as a new matrix to embed ceramic particles and replace the extensively studied WC-Co cermet system for high temperature. However, few of these studies deal with the evaluation of the different tribological properties and their relationship with the coating microstructure. In the present study, the near stoichometric Fe40Al was successfully sprayed by means of high velocity oxy-fuel using different particle size distribution and the tribological behavior was assessed through solid particle erosion, abrasive and dry sliding tests. The wear mechanisms of the deposited coatings are discussed with regard to the observed results. In addition, oxidized samples were tested to evaluate the role of the oxide top layer; also, the powder was previously annealed to produce a coating with an almost fully ordered FeAl structure.

Keywords erosion and abrasion resistance, friction and wear, HVOF microstructures, HVOF spray parameters, wear, wear mechanisms

1. Introduction

One of the current challenges in materials science is to find versatile materials able to withstand good resistance for different service performance situations. A combination of good mechanical properties, corrosion, oxidation, and wear resistance is usually difficult to reach.

Currently, intermetallic compounds (IMCs) are being investigated as a good compromise for the above requirements. They are regarded as advanced materials, attractive due to their unique properties: high melting points, great strength but poor ductilities. In these respects, they resemble ceramic materials. Unlike ceramics, however, they have a metallic lustre and conduct heat and electricity well. Thus, they have been exploited not only for their mechanical properties but their chemical, electrical, magnetic, optical, and semiconducting properties as well (Ref 1).

Although IMCs have been studied and employed over decades, their interest is relatively new and has been motivated by the demand of finding some sort of materials capable of substituting superalloys, especially for jet engine development (Ref 2, 3); their particular structure is the reason of their high stability. Whereas conventional alloys are defined by atoms linked with relatively weak metallic bonds, IMCs have either partly ionic/covalent bonds or, having entirely metallic bonds, the atoms take up preferred positions within the crystal lattice. Because of such atom arrangement, IMCs tend to have a much lower self-diffusion coefficient than do disordered alloys and so their structure can be maintained to high temperatures (Ref 4). Nevertheless, their long-range ordered superlattices reduce dislocation mobility and diffusion processes leading to their inherent embrittlement. It has been observed that some can even keep such order up to their melting point, otherwise they disorder below a certain critical temperature (T_c) at which an order-disorder transformation might occur.

Contemporary efforts have been addressed to aluminides of transition metals, i.e. Fe, Ni, Ti, Co, and Nb; these compounds possess relatively low densities, high specific modulus, high melting points, strength and excellent oxidation and corrosion resistance because of the formation of a protective alumina layer (Ref 5, 6). However, since the first investigations about intermetallics carried out by Kumakov et al. (1916), their low ductility has hampered their fabrication. To overcome such a handicap, many attempts have been carried out in the last decades to

This article is an invited paper selected from presentations at the 2008 International Thermal Spray Conference and has been expanded from the original presentation. It is simultaneously published in *Thermal Spray Crossing Borders, Proceedings of the 2008 International Thermal Spray Conference*, Maastricht, The Netherlands, June 2-4, 2008, Basil R. Marple, Margaret M. Hyland, Yuk-Chiu Lau, Chang-Jiu Li, Rogerio S. Lima, and Ghislain Montavon, Ed., ASM International, Materials Park, OH, 2008.

J.M. Guilemany, N. Cinca and **J. Fernández**, Thermal Spray Centre, University of Barcelona, Barcelona, Spain; and **S. Sampath**, Center for Thermal Spray Research, Stony Brook, New York. Contact e-mail: nuria.cinca@ub.edu.

enhance their ductility, such as reduction of grain size (Ref 7) or addition of certain alloying elements (Ref 8, 9).

Their difficulty to fabricate as structures has stimulated their use as coatings. In a previous study, the oxidation behavior of high velocity oxy-fuel (HVOF) sprayed FeAl coatings was already reported (Ref 10). Such aluminide (B2 ordered structure, CsCl-type) has a density of 5.56 g/cm^3, excellent sulphidation resistance, and good strength up to 600 °C (Ref 6, 11). Its applications include, among others, molten salt systems for chemical air separation, automotive exhaust systems, immersion heaters, heat exchangers, catalytic conversion vessels, chemical production systems, and coal conversions systems. Since some of the previous applications involve removal of material due to contact damage, few studies have recently evaluated their wear response either in bulk or coating form. Friction has been the most investigated mechanism and delamination was found to be the predominant cause for volume loss in coatings (Ref 12-14). The wear resistance was further improved by reinforcement with hard particles (Ref 13, 15). The presence of such particles has also been reported to affect the abrasive and erosion properties even for NiAl (Ref 15-17).

The other two wear mechanisms, mainly abrasion and erosion, have been studied for FeAl and NiAl coatings (Ref 18, 19). Alman et al. (Ref 14, 16) compared the wear rates of Fe-Al based alloys with those of other metals and ceramics and concluded that their resistance was as much as that encountered in typical austenitic stainless steels. Moreover, the higher the Al content, the further the wear rate decreased relating to bulk hardness of the compound.

Ordering in these compounds is also induced by heat treatments to yield B2 (36-48 at.% Al) or $D0_3$ (interpenetrating FCC lattices, composition range 23-36 at.% Al and from room temperature to 550 °C) ordered structures (Ref 20), which result in lower wear rates compared to these non-long-range ordered iron aluminides (Ref 21, 22).

The present study intends to assess all the above wear responses for FeAl intermetallic coatings based on different microstructures. A main comparison is reported concerning two different microstructures obtained by using different particle size distribution; secondly, the effect in lattice ordering is assessed by previously annealing the feedstock powder and, finally, thermal oxidation is intended to evaluate how surface modification would affect to wear properties.

2. Experimental Procedure

The FeAl powder alloy namely Grade 3, provided by CEA-DTEN (*C*ommissariat à l'*E*nergie *A*tomique – *D*epartement de *T*echnologie des *E*nergies *N*ouvelles, Grenoble) and Mecachrome (Vibraye, France) (Ref 23), was used to produce the FeAl coatings onto low alloyed carbon steel substrate. The powder with an initial composition of Fe40Al-0.05Zr (at.%) + 50 ppm B was prealloyed by gas atomization and subsequently ball-milled. Boron and zirconium were introduced as alloying elements to improve ductility in the material (Ref 9, 24, 25) and yttria (ODS, oxide dispersed strengthening) was added during the milling step in order to keep fine grain size after hot consolidation and forming so that mechanical strength (Hall-Petch mechanism) and room temperature ductility (reduction of the environmental embrittlement caused by water vapor at RT thanks to grain size reduction down to 1 μm) are improved (Ref 26-28).

CEA-DTEN was the first supplier and it was afterwards transferred to Mecachrome. Both suppliers provided the same powder with the same composition but with the respective powder distributions as observed in Fig. 1. The whole CEA-DTEN powder distribution was used to produce the coating which will be referenced as

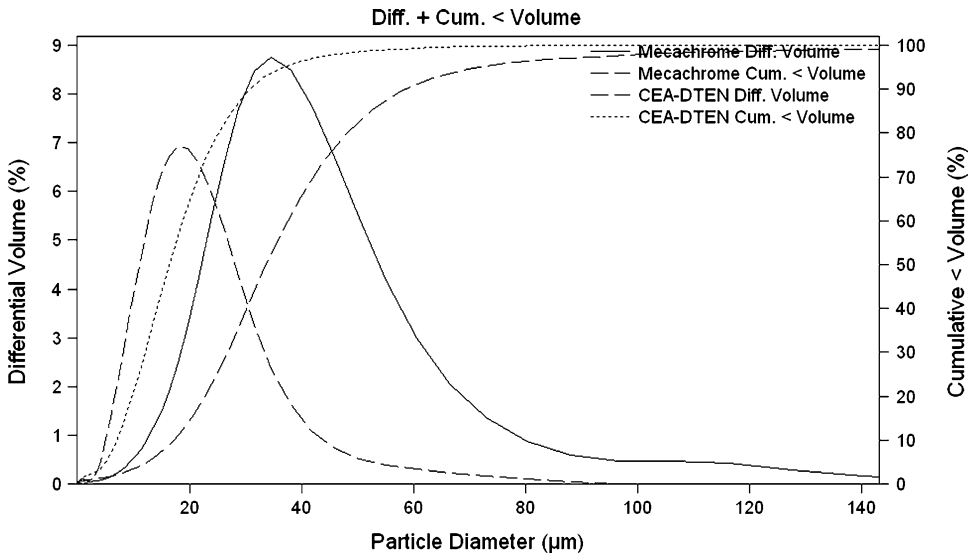

Fig. 1 Powder size distribution

Table 1 Thermal spraying parameters

	FeAl
Oxygen flow rate, L/min	189
Propylene flow rate, L/min	87
Carrier gas, L/min	305
Oxygen/fuel ratio	2.874
Feeding rate, g/min	20
Spraying distance, mm	250

CEA, while from the 40-60 μm fraction, the one referenced as MEC40-60 was obtained. Furthermore, a third coating was produced by spraying the 40-60 fraction size being annealed at 700 °C for 10 min in order to induce the ordering in the intermetallic structure and then evaluate the properties of the resulting coating compared to that of MEC40-60 (this will be referenced as MEC40-60$_{ANN}$). The annealing treatment was carried out in a controlled atmosphere furnace with a continuous argon flux.

A Diamond Jet Hybrid gun model 2600/2700 was employed for powder deposition, and Table 1 presents the spraying parameters. Such parameters were previously optimized with the intention to achieve the less oxidation content as possible (Ref 29).

The CEA coating was oxidized at 900 °C for 72 h (referenced as CEATT). The selection of the temperature for the treatment was based on a previous study where the formation of an adherent oxide scale was shown (Ref 10). The idea came from the work carried out by Xia et al. (Ref 30) who claimed that the average wear rate is reduced 16 times when the bulk intermetallic is compared with an untreated specimen. Both the microhardness of the as-sprayed and the oxidized coatings were investigated using a Vickers indentation tester MATSUZAWA MXT-a at 200 gf load for 15 s in the cross sections. At least 20 indentations were performed for average.

For the microstructural cross sections and top surfaces characterization, a JEOL scanning electron microscope (SEM) was used with energy dispersive spectroscopy (EDS) for microanalysis. X-ray diffraction (XRD) scans helped to identify the phases present after the spraying process. In addition, the ''image analysis'' option within the Matrox Inspector 1.71 software was employed for the oxidation and porosity evaluation. This was done by taking a micrograph of the overall coating cross section; at least 10 pictures were analyzed like this for each coating.

2.1 Abrasive Tests

According to ASTM G65-00, the Rubber Wheel test consists of a rubber wheel rotating at a constant speed of 139 rpm on the specimen while silica particles (particle size in the range of 0.4-0.8 mm) flow by gravity between the two contacting surfaces. The samples were tested in their as-sprayed state.

A normal load of 50 N is applied and the mass loss is measured up to 30 min. The abrasion wear rate W ($mm^3\ N^{-1}\ m^{-1}$) is calculated as:

$$W = \frac{\Delta m}{t}\frac{1}{N}\frac{1}{\rho} \quad \text{(Eq 1)}$$

where Δm is the average mass loss (g), t is the test time (min), N is the normal load, and ρ (g cm^{-3}) is the FeAl powder density calculated as follows: a known mass of powder is introduced into a 25 mL flask and is filled with a high wettable liquid with a known density, here cyclohexanone.

$$\rho = \frac{m_p}{\left(25 - \frac{m_T - m_p}{\rho_{liq}}\right)} \quad \text{(Eq 2)}$$

where m_p is the mass powder introduced, m_T is the total mass (powder + cyclohexanone), and ρ_{liq} is the cyclohexanone density at working temperature.

This methodology for calculating the density has been considered a much better approximation to the real value of the material than vibrated and tap densities referenced according to ASTM B-212 and ASTM B-527, respectively. Although it is evident that both coatings do not have the same density, powder density has just been used as approximation.

2.2 Erosion Tests

The erosion tests have been performed at room temperature using a grit-blasting apparatus. The Al_2O_3 abrasive particles whose average size is about 50 μm leave the nozzle at the velocity of 1 g/min controlled by selecting the air pressure at 10 psi (regularly checked by weighting the alumina collected for 1 min). The nozzle tube was 1.5 mm inner diameter and 50 mm long.

The sample's dimensions were 20 × 20 × 5 mm and, before testing, they were polished down to 1 μm. The distance from the specimens surface to nozzle end was 10 ± 1 mm and the angle between the nozzle axis and the specimens surface was 90°. The mass loss was obtained by weighting on an analytical precision balance every 30 s and the test was stopped when the substrate was reached.

The average erosion value of the coatings was calculated by dividing erosion rate (g min^{-1}) by the abrasive flow rate. It is then normally divided by the specimen density (powder density, g cm^{-3}) and the average value is then reported as $mm^3\ g^{-1}$.

2.3 Dry Sliding Behavior

Friction tests were carried out with a ball-on-disc system according to ASTM G99-03, where an 11 mm diameter WC-6Co ball was frictioning the polished coating surface (below 0.8 Ra). A temperature around 25 °C and the humidity (below 20%) were controlled during the test time into the closed camera where the experiments were performed. A sliding speed of 0.11 m/s, track diameter of 16 mm, and sliding distance of 1000 m were constant for all the tests. The variation of friction coefficient with sliding distance was registered at 5 N for the FeAl coatings and a comparison with the wear behavior of the steel substrate and the thermal treated sample is given.

According to the standard, the friction coefficient (FC) is given as the average of the values obtained for the last 200 m.

The volume loss was obtained by means of white light interferometry (SWLI). The interferometric surface analysis microscope (Zygo New View 100) uses SWLI to image and measure tested surfaces and provide surface analysis without contacting it. Depths up to 100 μm, with 0.1 nm resolution and 0.3 nm RMS repeatability, are imaged independently of the objective magnification; lateral resolution is 500 nm. SWLI is a technique based on the constructive or destructive interferences of two light beams, one going to a reference and the other to the sample, which leads to the obtention of a 3D image with the profile of the wear track.

The wear rate K ($mm^3\ N^{-1}\ m^{-1}$) is calculated as:

$$K = \frac{V}{ws}, \qquad \text{(Eq 3)}$$

where V is the worn volume, w (N) is the normal load, and s (m) is the total distance.

The as-sprayed coatings were characterized by SEM and microhardness indentation. The worn surfaces were also examined using SEM-EDS.

3. Results and Discussion

3.1 Coating Deposition and Characterization

Figures 2(a) and (b) show the SEM and XRD morphology of the powder. X-ray presents the typical fundamental lines of the FeAl pattern (h + k + l = even), being only exhibited when the structure is disordered as, otherwise, the superlattice lines (h + k + l = odd) would also appear; this was already foreseen as result of the high plastic deformation induced by ball-milling. It is even worth noting that the peak broadening comes from the finer grain size and microstrain introduced during milling. By contrast, when the powder is annealed, the X-ray presents the superlattice peaks conserving a slight broadening, which means that after the annealing treatment the structure has been partly reordered (Fig. 2b).

Using different particle distributions, a great difference was observed on the resulting microstructures (Fig. 3a and b). Whereas MEC40-60 mainly consists of partially melted particles with some porosity and an oxide layer at the interparticle zones, CEA is well featured by partially and fully melted particles with some light and dark-grey contrasts at the intersplats boundaries. These have been characterized as iron-rich and oxide zones by EDS, respectively; the presence of Al-depleted regions suggests that during spraying, oxidation has occurred to the powder to form the Al-rich spinel $FeAl_2O_4$ oxide leaving Fe-rich areas at the lamellar boundaries. XRD also confirms the former results (Fig. 4); the additional peaks also identified as FeAl correspond to the superlattice lines; some authors have attributed their presence to the ordering within the

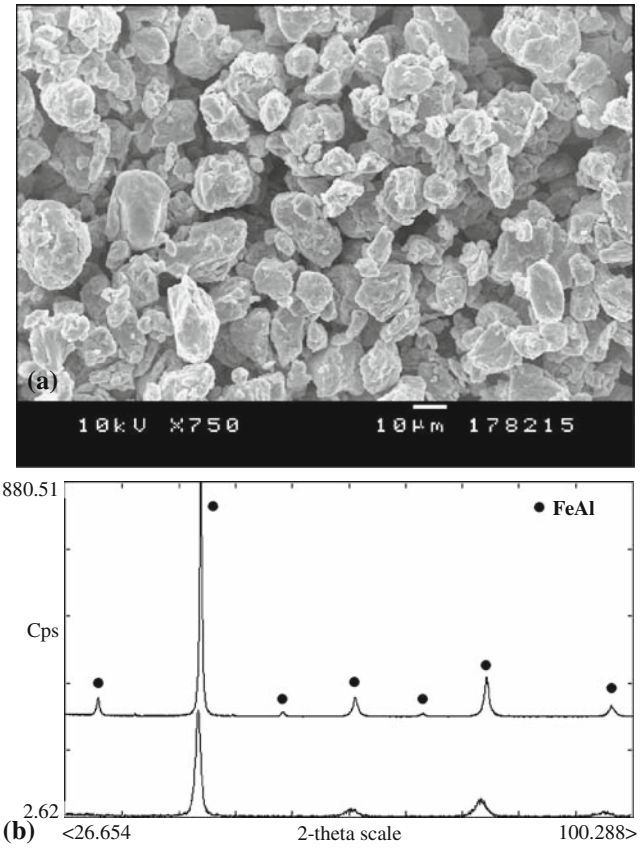

Fig. 2 (a) Morphology and (b) X-ray of the iron aluminide powder grade 3 as-supplied and annealed at 700 °C

melted areas (Ref 31). The difference in both microstructures can be easily observed also by the examination of the fracture sections (Fig. 5 and 6). Figure 5 illustrates the CEA coatings being built up by melted splats aggregation, while Fig. 6(a) and (b) do not exhibit such morphology and one can see two features: one where a particle has been torn off, and the other where the particle still remains in that part of the coating. Coating thicknesses, as well as porosity and oxide contents, are presented in Table 2; they point out the difference between the two coatings and the features that have been discussed. MEC40-60_{ANN} is not illustrated here as it shows an analogous structure as MEC40-60.

By contrast, oxidized CEA presents a microstructure as shown in Fig. 7(a), where it can be seen that a very thin layer has been formed on the top. Although not being pure alumina as commonly found for bulks, the oxide characteristics are good enough to provide a good corrosion resistance; otherwise an easy oxygen inward diffusion would have produced an increase in oxidation kinetics. Such good performance has been associated to the presence of Al_2O_3 nuclei among the Fe_2O_3 nodules that prevent their growth. The X-ray spectrum indicates the presence of the before mentioned phases (Ref 10) (Fig. 7b).

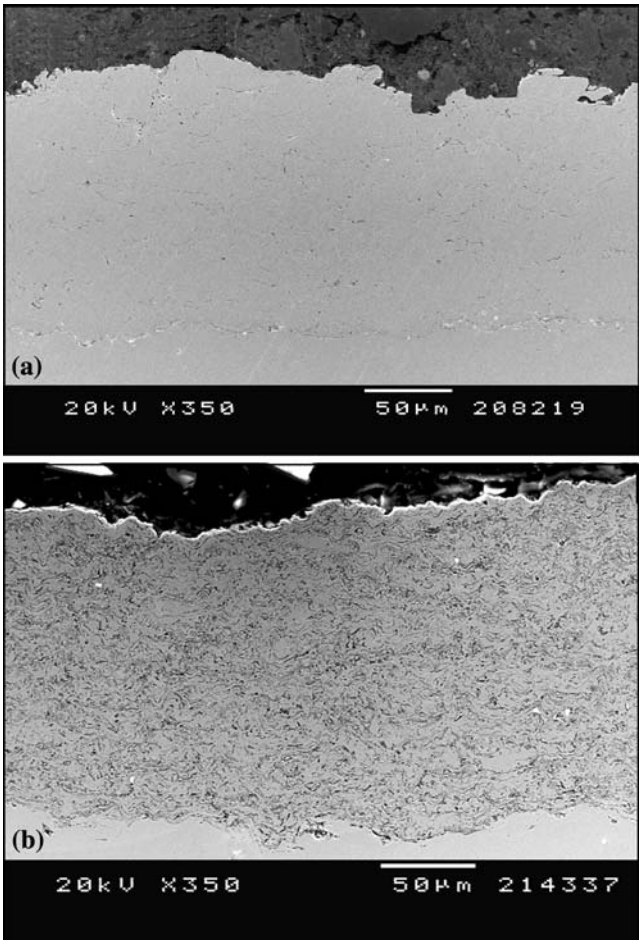

Fig. 3 SEM cross sections of (a) MEC40-60 and (b) CEA

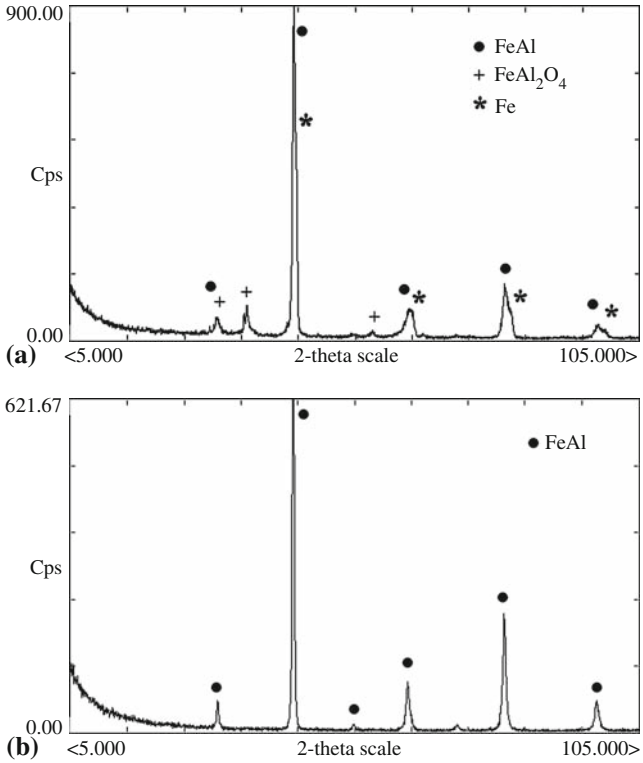

Fig. 4 XRD of (a) CEA and (b) MEC40-60 coatings respectively

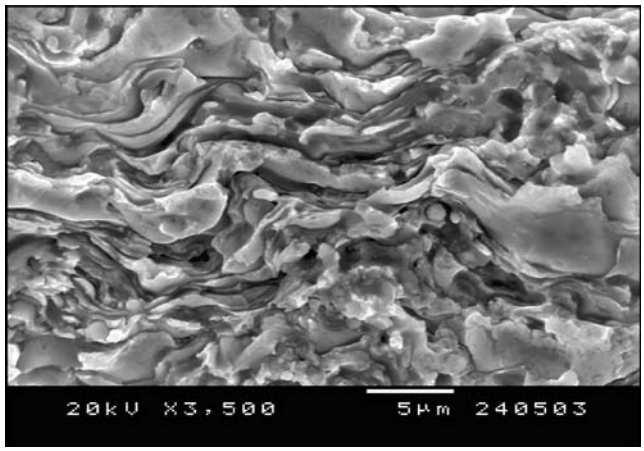

Fig. 5 Fracture section of the CEA coating

Regarding the microhardness values (Table 3), it can be seen that despite having different porosity levels, the overall presence of oxidation in CEA produces an increase in hardness as well as an embrittlement compared to MEC40-60. In addition, it might be associated to the higher occurrence of intersplat boundaries; in CEA, the indentation has more probabilities to include representative features of the overall coating structure, whereas in MEC40-60 the indentation might be performed inside an unmelted particle.

The comparison between the hardness values of MEC40-60 and MEC40-60$_{ANN}$ can be discussed as follows: as a consequence of not having the stoichiometric 50:50 FeAl and even more, having a milled strained structure, the lattice must present constitutional defects; according to Jordan and Deevi (Ref 32), vacancy hardening can ameliorate hardness and strength of iron aluminides but is detrimental to room temperature ductility. Although the cooling rate during the deposition process might also have a considerable influence on the vacancy concentration (Ref 33-35), the main difference between the two coating structures is the fact that annealing the feedstock powder might have eliminated most of the defects produced by milling and has ordered the lattice; therefore, from this point of view, there has been a strain release and the logical conclusion would be that lowering vacancy defects should lead to a less hard deposit. Nevertheless, the reason why this does not occur must find answer assuming that some oxidation might have occurred during the annealing process, even though it was carried out in argon atmosphere as some powder particles seemed to have a different color tonality.

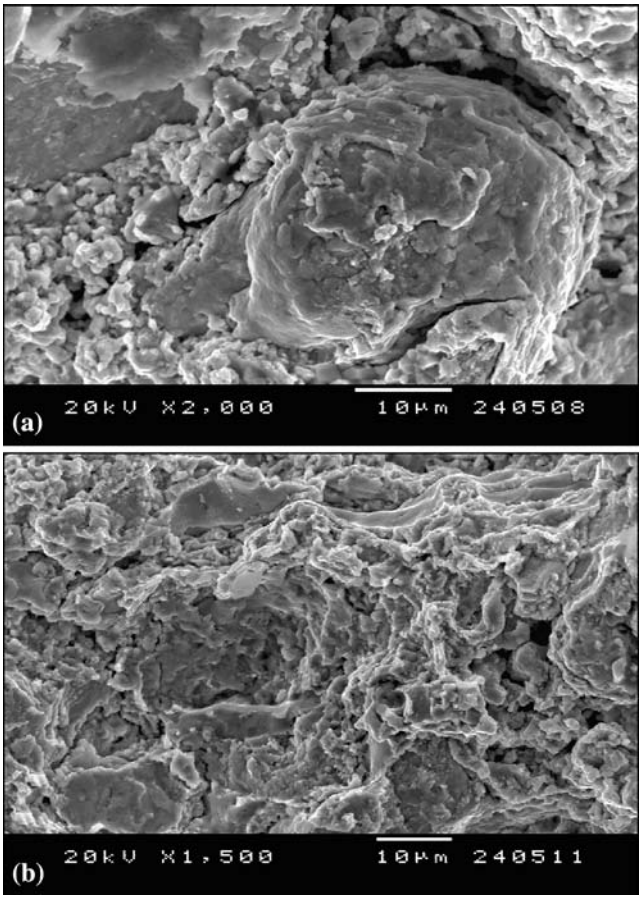

Fig. 6 (a, b) Different zones of the fracture section of the MEC40-60 section

Table 2 Coating features

	Thickness	% Oxidation	% Porosity
CEA	162 ± 6	13.4 ± 2.6	1.8 ± 0.1
MEC40-60	147 ± 9	4.4 ± 0.6	0.3 ± 0.1

Furthermore, with regard to CEATT, looking at the standard deviation, HV differences between CEA and CEATT are not really significant.

3.2 Abrasive Tests

The present work examines a three-body abrasive wear, where silica particles are introduced and flow by gravity between the two surfaces (rubber rotating wheel and the as-sprayed coating). This kind of wear involves plastic deformation whenever the coating hardness is lower than $H_a/1.2$, where H_a is the hardness of silica particles; otherwise, the abrasive particles would smash (Ref 36). In the case of all studied coatings, $H_a/H_c > 1.2$ (hard abrasion) was observed to cause plastic scratching.

In a previous study, the abrasive behavior was already discussed for the as-called CEA coating (Ref 29). Compared to the others, CEA exhibits the highest abrasive

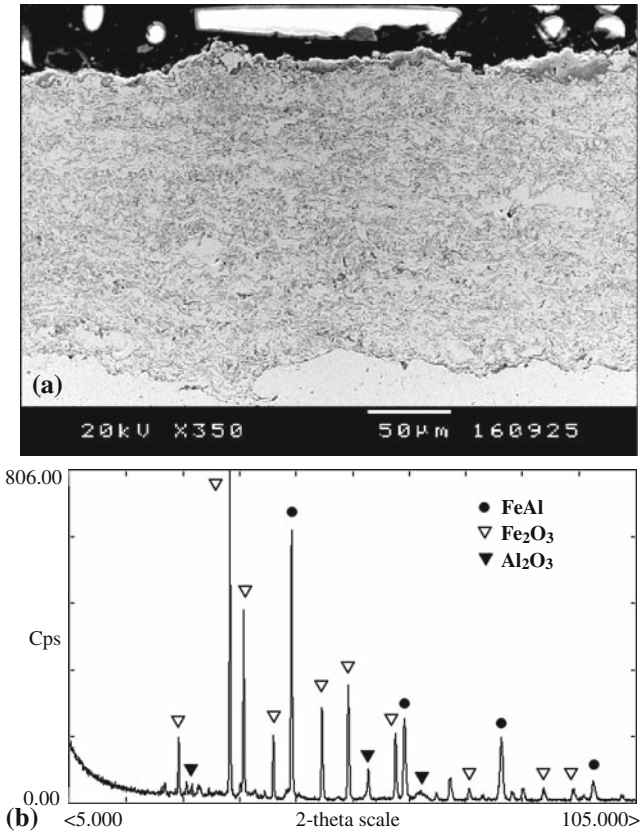

Fig. 7 (a) SEM cross section and (b) X-ray of CEATT

wear resistance, which is assumed to be due to its highest hardness (Table 4). Hence, the harder the coating is, the less damage is produced by abrasive silica particles as a harder coating reduces wear by preventing ploughing on both a macro and micro-scale. Abrasive wear has also been found to be dependent on crystal structure and orientation; Alison (Ref 37) showed that cubic metals wear at about twice the rate of hexagonal metals, which was attributed to the lower work-hardening rate of the hexagonal metals. This reasoning serves also to discuss that the ordered FeAl lattice ($MEC40\text{-}60_{ANN}$) is less work-hardened than the disordered structure (MEC40-60).

Figure 8 shows the wear rate along the test time. The noticeable rapid initial decrease in the oxidized CEA is attributed to removal of the oxide surface layer; an examination of both damaged surfaces, that of the as-sprayed CEA and the oxidized one, indicates that the as-sprayed coating shows the grooves the hard silica particles have produced during the test, whereas the oxidized coating shows the cracks produced on the oxide scale. Such scale is not enough homogeneous to protect the coating against ploughing. Moreover, the fractured oxide debris can produce a more aggressive three-body abrasive effect.

The additions of hard particles such as TiC or TiB_2 in a Fe_3Al or FeAl matrix have been shown to reduce the wear rate by an order of magnitude. Such improvement has been also claimed by some authors (Ref 38, 39) who focused on

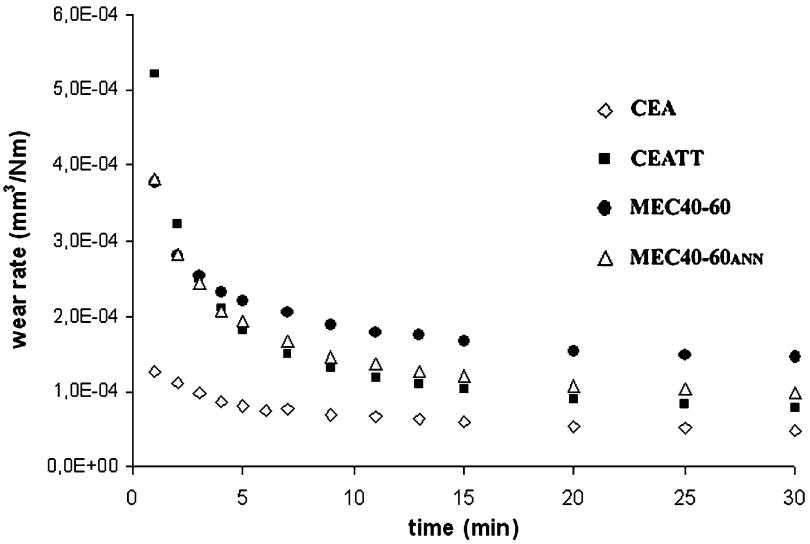

Fig. 8 Mass loss (g/min) versus time

Table 3 Microhardness of intermetallic FeAl coatings

	HV_{200}
CEA	434 ± 48
CEATT	426 ± 23
MEC40-60	377 ± 36
$MEC40\text{-}60_{ANN}$	415 ± 21

Table 4 Abrasive wear rates

	Wear rate, $mm^3\ N^{-1}\ m^{-1}$
CEA	3.7×10^{-5}
CEATT	5.2×10^{-5}
MEC40-60	1.2×10^{-4}
$MEC40\text{-}60_{ANN}$	6.7×10^{-5}

the comparison of the use of this intermetallic instead of usual Co as matrix. Interestingly, they stated that WC-40%FeAl exhibits similar wear resistance to that of commercial WC-10%Co. Particularly, FeAl ordered matrix is attractive for wear resistance in high-temperature environments.

However, there is not an extensive study on the abrasion resistance of thermally sprayed FeAl coatings and even in the case of their comparison to other deposited materials, the conditions they have been tested with, are not always comparable.

What can be actually compared are the present results with that of other materials tested with the same equipment and following the same standard. NiCr-based coatings exhibit wear rates of the same magnitude as MEC40-60, whereas CEA and CEATT are one order of magnitude lower because of the higher hardness (Ref 40). WC-12Co, for instance, showed a wear rate in the order of 10^{-6} $mm^3\ N^{-1}\ m^{-1}$ (Ref 41).

3.3 Erosion Behavior

With regard to test variables, in abrasive wear, the amount of material removed depends on the normal load pressing the particles against the surface and on the distance slid. In erosion, however, the extent of damage mainly depends on the number and mass of individual particles striking the surface, and on their impact velocity. As in the case of abrasion, mechanisms by which a metallic material is removed can involve both plastic deformation and brittle fracture; they can either depend on erodent particle sizes, velocities, impact angles, or environments. Hence, if plastic deformation dominates, the maximum wear occurs at low angles (''ductile behavior''), while at high impact angles erosion by brittle fracture is more rapid (''brittle behavior''). Striking at low angles with rounded particles normally yields to surface ploughing, whereas using angular particles produces cutting (Ref 42). At 90°, the damage normally occurs by cracking and chipping of surface material; in the case of coatings, this is favored by low strength of inter-lamella.

Figure 9 shows one of the damaged surfaces, which is clearly associated to the eroding effect of angular shaped particles where the material is displaced forming rims or lips. It is worth noting that such a mechanism, known as *cutting*, is normally encountered in ductile mechanisms (more attributed for metals at low impingement angles). However, the angular dependence of erosion is not a characteristic of the material alone, but depends also on the conditions of erosion. Thus, there can be alloys that erode in a ''brittle behavior'', that is, alloys of high hardness and low ductilities that show their maximum erosion rates at normal incidence. The terms ''brittle'' and ''ductile'' in erosion context must be then used with caution (Ref 42). Wang et al. (Ref 18, 43) also claimed that; in their results, the eroded surfaces also appear to result from a ductile mechanism. Few studies report their results on erosion performance of FeAl coatings; nevertheless,

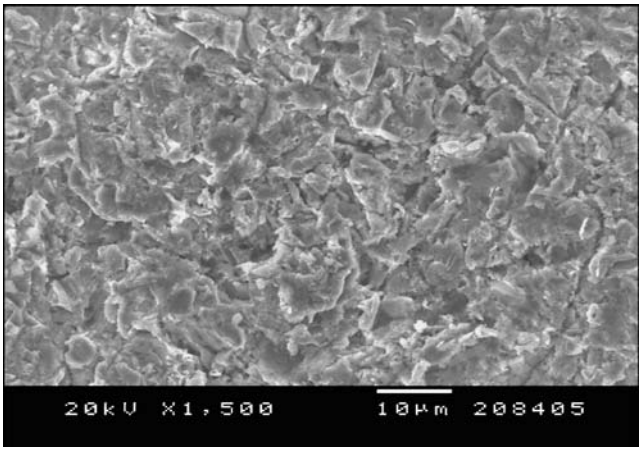

Fig. 9 Erosion surface morphology

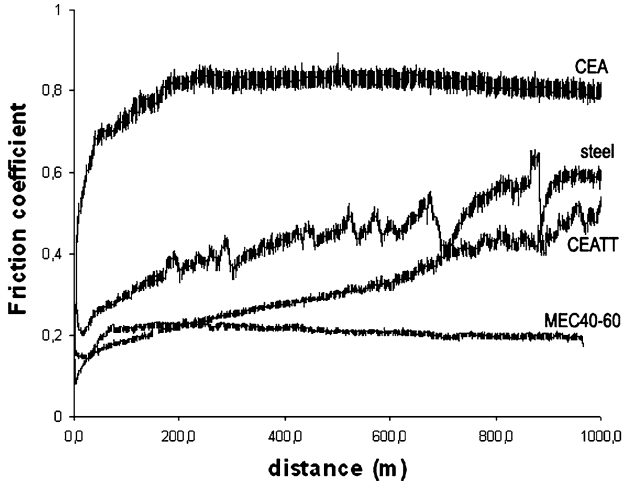

Fig. 10 Friction coefficient versus sliding distance

Table 5 Wear rates of the eroded surfaces

	CEA	MEC40-60
Wear rate, $mm^3\ g^{-1}$	2.42×10^{-4}	2.09×10^{-4}

those carried out on NiAl intermetallics also support the former evaluation (Ref 18, 44). The addition of ceria has shown to ameliorate significantly the erosion resistance (Ref 43).

Table 5 shows the wear rates having MEC40-60 slightly higher erosion resistance than CEA. This cannot be understood from the reasoning of hardness material as in abrasive wear. There is normally an inverse relationship between wear and hardness. In the most simple way, assuming a single particle striking the surface with mass (m), the work done by the retarding force will be equal to the initial kinetic energy of the particle (v_0), resulting in a final indentation volume (V) (Ref 42):

$$V = \frac{mv_0^2}{2H} \qquad \text{(Eq 4)}$$

Even more complex theoretical models predict that erosion rates mainly involving plastic deformation should be inversely proportional to the hardness of the material. However, when using H in the equations, the fact that the material at the worn surface is strain-hardened by plastic flow is ignored, as well as the consequence that its hardness will generally be greater than that of the unstrained material; therefore, better correlation is found between wear resistance and the hardness of the worn surface. It is assumed then that as result of the different microstructures the material is more or less strain hardened (Ref 42). It might be also said that the cohesion between splats in the CEA specimen is not as high as in MEC40-60, maybe because of the presence of much more porosity and oxide embrittlement. It can be compared with difficulty to other investigations because of the different parameters set chosen in each study.

Before choosing the ones established in the present work, there were tested those corresponding to G76-04 ASTM standard but they were discarded for being so aggressive for the coatings.

3.4 Dry Sliding Behavior

Figure 10 shows the variation of friction coefficient versus sliding distance at a normal load of 5 N for the steel substrate and the different coating systems as well. While the FC of the non-coated sample increases continuously during the entire test, the FC of the CEA coating shows the following trend: in the early minutes, there is a sharp increase and then it rapidly reaches a steady state at about 0.7, which persists during the rest of the test. However, the oxidized sample exhibits a different behavior slightly increasing during the whole test and showing some fluctuations at the end. MEC40-60 and MEC40-$_{60ANN}$ show, by contrast, surprisingly much lower friction coefficient. A common trace of all these plots is the initial raise, which is associated to the high adhesive contact between the WC-Co counterpart material and the coating material; the slight decrease afterwards may be caused by the hardening effect under the compressive stress the material undergoes.

In the case of similar microstructures but different hardness, lower friction coefficients would have been achieved with the hardest coating. Lower friction indicates that lower shear has taken place and therefore contact area is much smaller. This can be explained by the examination of the wear tracks.

Figures 11-13 show the common features of damaged coatings and Table 6 gives the magnitudes of their respective widths as well as the volume loss and the calculated wear rates. SWLI had not enough resolution to detect MEC40-60 track's depth.

The magnification in Fig. 11 shows the plate-like debris on the worn CEA surface consisting of ploughed portions caused by adhesive mechanism and posterior delamination. EDS analysis indicated that oxidation takes place on the fresh coating when the ball slides over the deposit

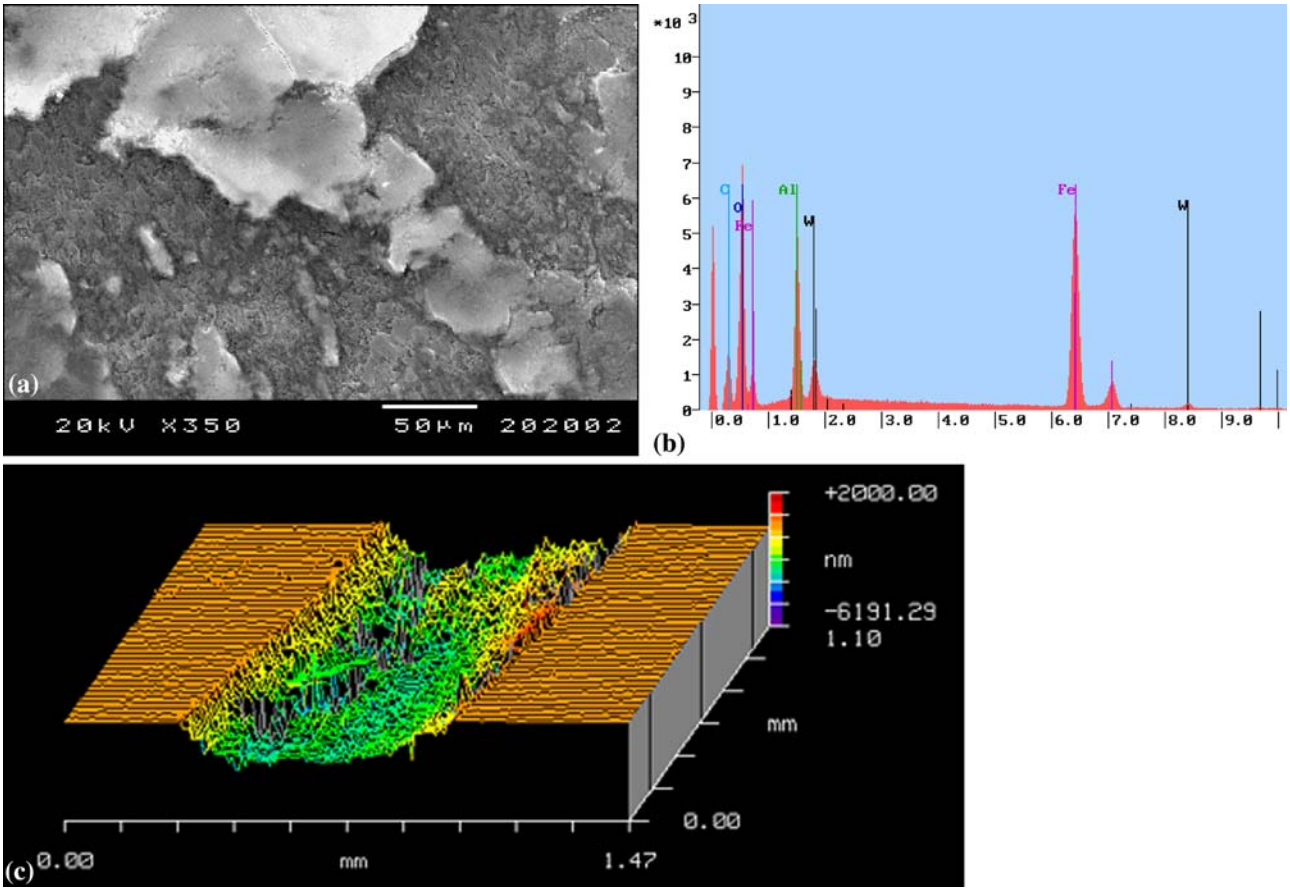

Fig. 11 (a) Wear debris after the ball-on-disk test on the CEA sample, (b) EDS analysis on the plate-like debris, and (c) wear track profile

(Fig. 11b). Such oxidation may be explained by the temperature rise during friction contact. Moreover, the debris observed in the laterals of the wear track could also play some role on constraining laterally and making easier the deformation of the central layer. The debris also entrapped between the two surfaces could have also caused more severe damage in CEA.

Friction coefficients are calculated as an average value of the last 200 m. Although there is a fluctuation for CEA TT and steel substrate, according to the standard, these would then result in 0.50_6 and 0.59_1, respectively. In the other cases, that value is more reliable as a uniform stage is reached.

Unlike CEA, which shows delamination as also reported by other authors (Ref 45), the as-thermally treated and MEC40-60 exhibit completely different wear mechanisms. Figure 12 corresponds to the wear track of the oxidized sample which is covered by an oxide layer of several microns as shown in the cross section in Fig. 12(b) (this is the reason why volume increment is expressed as a positive value, because it is above the surface plane). The thin and brittle layer corresponds to alumina as demonstrated by EDS. It could be thought that it could have a lubricant role as well as the oxidation debris in CEA, but it seems that the continuous break-away of such oxide layer, being alternatively formed and detached from the fresh coating, produces the non-uniformity in the friction coefficient. Xia et al. (Ref 30) claimed that a uniform FC value was maintained in their oxidized samples along the whole test. Nevertheless, as they underwent the study in compacted FeAl grade 3 specimens, the wear mechanism was not the same as that of a coating such as CEA. FC graphics are more similar to MEC40-60 because that had a microstructure similar to a bulk sintered material.

Sliding behavior has also been evaluated by Xu et al. (Ref 12, 13) with FeAl HVAF (High Velocity Air Fuel) coatings, which exhibited a microstructure similar to that of CEA with melted particles and oxidation in the inter-lamellas. After performing pin-on discs at 3, 5, and 7 N, they concluded that when load is increased, friction leads to lower FC owing to the presence of a similar oxide film as that encountered in CEA. However, what these authors did not try was to change spraying conditions in order to ameliorate wear response. In the present study, the MEC40-60 coating significantly shows an improvement. MEC40-60 possessed the lowest friction coefficient, no delamination was found but the wear track was identified by some remaining oxidation at both sides (Fig. 13). Splat delamination observed in CEA is commonly associated to the weak bonding between lamellas. Also, porous,

oxides-sprayed material interfaces, and other imperfections behave as stress concentrators that serve as trigger factors to yield crack initiation. Therefore, it is difficult to predict how a thermal sprayed deposit will behave at friction dynamic contact and often complex simulations are needed; only hypothesis can be made depending on the microstructure obtained. Hence, the absence of these many defects in MEC40-60 is the key for improvement. Here, the annealing treatment of the powder seems not to have a strong influence on the friction behavior, indicating that the wear mechanism is more influenced by the microstructure rather than the hardness of the material itself.

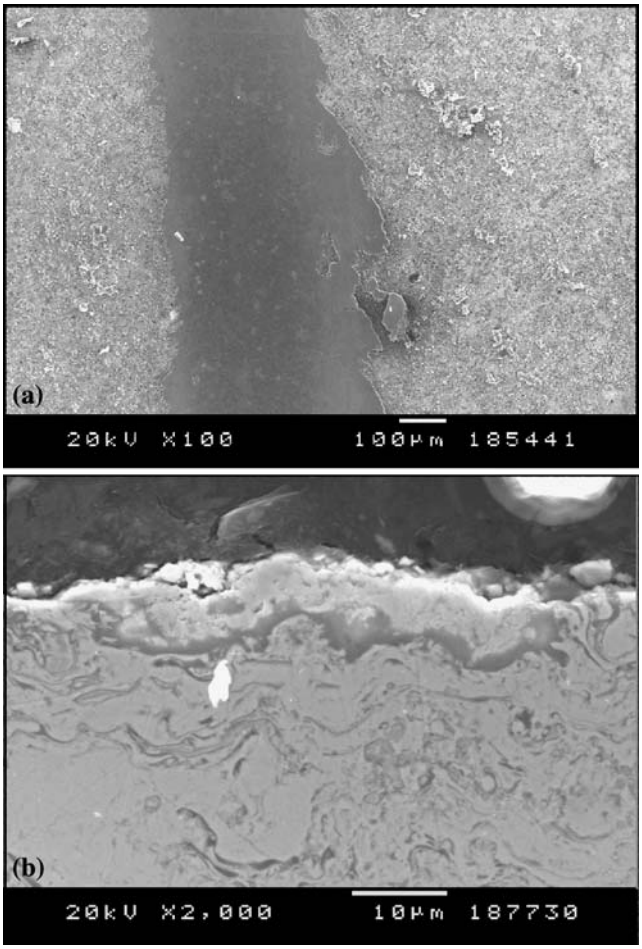

Fig. 12 (a) Wear track observed on the oxidized CEA coating and (b) cross section of the oxide layer formed after the sliding test

As already discussed in terms of erosive and abrasive behavior, sliding behaviour has also been compared with other HVOF-coating materials tested under the same conditions. Thus, when volume loss is compared (mm^3 normalized for the whole perimeter) with a cermet WC-metal coating, the damage produced in CEA is as high as two order of magnitudes more (Ref 15, 17). More similar friction coefficients were obtained with NiCr-based coatings (Ref 16).

4. Conclusions

The results of the present work can be summarized as follows:

- Two very different coatings were obtained from the same powders just modifying the particle size for spraying. This resulted in different microstructures: CEA is dominated by almost fully melted particles surrounded by iron-rich and oxide phases, while MEC40-60 is similar to a bulk material where particles have been compacted.
- Different hardness coatings yield to different abrasive wear rates, where CEA showed the higher abrasive resistance.
- The difference between MEC40-60 and MEC40-60_{ANN} hardness has been associated to the internal oxides rather than to the lower vacancy defects produced during annealing the powder. Both, milling conditions from the as-atomized powder and quenching effect

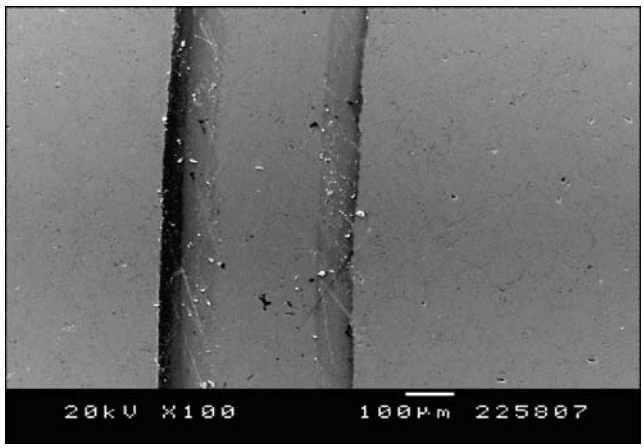

Fig. 13 Wear track of the MEC40-60 coating

Table 6 Wear track features

	CEA	CEATT	MEC40-60	MEC40-60_{ANN}
Friction coefficient	0.706	0.506	0.192	0.190
Track width, µm	579 ± 8	361 ± 15	377 ± 26	375 ± 20
ΔV, mm^3	-3.3×10^{-2}	$+1.6 \times 10^{-2}$	…	…
Wear rate, $mm^3\ N^{-1}\ m^{-1}$	5.9×10^{-6}	3.6×10^{-6}	…	…

produced during the spraying process, have been identical for both powders; thus, knowing that stress release would reduce hardness, oxidation during the annealing treatment must have enhanced the hardness.

– Erosion tests demonstrated that iron aluminides possess a ductile behavior even when the impingement angle is 90°, which is normally usual of brittle mechanisms.
– Ball-on-disc tests were analyzed in terms of different microstructures and it was stated that CEA was worn by delamination, whereas MEC40-60 almost does not suffer any damage. The first one exhibits FC more than three times higher than the second one.
– Oxidation of the coating was unfavorable for its wear properties. The formation of the alumina layer when frictioning would have displayed a good role if it would not have been so brittle that its fracture left fresh coating areas ready to be damaged further.
– A good goal of this work has been the idea of previously annealing the powder; MEC40-60$_{ANN}$ shows an analogous microstructure as that of MEC40-60 but higher hardness and abrasion resistance while maintaining the same friction coefficient trend.

Acknowledgments

N. Cinca would like to thank to the Generalitat de Catalunya—project 2005SGR00310—and the Ministerio de Educación y Ciencia for the project MAT2006-06025 for the economical support and the researcher grant with reference number AP-2004-2453.

References

1. J.H. Westbrook, Applications of Intermetallic Compounds, *MRS Bull.*, 1996, **21**(5), p 26-28
2. K. Savolainen, J. Mononen, R. Ilola, and H. Hänninen, *Materials Selection for High Temperature Applications*, Helsinki University of Technology
3. R. Tanaka, Research and Development of Ultra-High Temperature Materials in Japan, *Mater. High Temp.*, 2000, **17**, p 457-464
4. P. Adeva, Materiales alternativos de las superaleaciones: compuestos intermetálicos, *Revista de la Asociación Española de Científicos*, 1999, **1**, p 1-6
5. S.C. Deevi and V.K. Sikka, Nickel and Iron Aluminides: An Overview on Properties, Processing, and Applications, *Intermetallics*, 1996, **4**, p 357-375
6. C.T. Liu and J.O. Stiegler, *Ordered Intermetallics. Properties and Selection: Nonferrous Alloys and Special Purpose Materials*, 10th ed., Metals Handbook, ASM International, 1990
7. H. Skoglund, M. Knutson, and B. Karlsson, Processing of Fine-Grained Mechanically Alloyed FeAl, *Intermetallics*, 2004, **12**, p 977-983
8. S.C. Deevi, V.K. Sikka, and C.T. Liu, Processing, Properties and Applications of Nickel and Iron Aluminides, *Prog. Mater. Sci.*, 1997, **42**, p 177-192
9. C.T. Liu, E.P. George, P.J. Maziasz, and J.H. Scneibel, Recent Advances in B2 Iron Aluminide Alloys: Deformation, Fracture and Alloy Design, *Mater. Sci. Eng. A*, 1998, **258**, p 84-98
10. J.M. Guilemany, N. Cinca, S. Dosta, and C.R.C. Lima, High Temperature Corrosion of Fe-40Al Coatings, *Intermetallics*, 2007, **15**, p 1384-1394
11. G. Sauthoff, State of Intermetallics Development, *Mater. Corr.*, 1996, **47**, p 589-594
12. B. Xu, Z. Zhu, W. Zhang, and S. Ma, The Microstructure and High-Temperature Sliding Wear Behavior of Fe-Al Coating Produced by High Velocity Arc Spraying, *Thermal Spray 2004: Advances in Technology and Application*, ASM International, May 10-12, 2004, Osaka, Japan, 2004, p 1129
13. B. Xu, Z. Zhu, S. Ma, W. Zhang, and W. Liu, Sliding Wear Behavior of Fe-Al and Fe-Al/WC Coatings Prepared by High Velocity Arc Spraying, *Wear*, 2004, **257**, p 1089-1095
14. J.A. Hawk and D.E. Alman, Abrasive Wear of Intermetallic-Based Alloys and Composites, *Mater. Sci. Eng. A*, 1997, **239-240**, p 899-906
15. M. Shi-ning, H. Jun-zhi, C. Xue-rong, L. Chang-qing, L. Qian, and J. Hai, Erosion Resistance of Arc Spray Composite Coatings at High Temperature on Boiler Tubes of Pulverixed Coal Fired Power Station, *Thermal Spray 2003: Advancing the Science and Applying the Technology*, B.R. Marple and C. Moreau, Eds., May 5-8, 2003, Orlando, FL, ASM International, 2003, Vol. 1: p 845; Vol. 2, p 864
16. D.E. Alman, J.A. Hawk, J.H. Tylczak, C.P. Dogan, and R.D. Wilson, Wear of Iron-Aluminide Intermetallic Alloys and Composites by Hard Particles, *Wear*, 2001, **251**, p 875-884
17. B. Wang and S.W. Lee, Erosion-Corrosion Behaviour of HVOF NiAl-Al_2O_3 Intermetallic-Ceramic Coating, *Wear*, 2000, **239**, p 83-90
18. Y. Wang and M. Yan, The Effect of CeO_2 on the Erosion and Abrasive Wear of Thermal Sprayed FeAl Intermetallic Alloy Coatings, *Wear*, 2006, **11-12**, p 1201-1207
19. J.A. Hearley, J.A. Little, and A.J. Sturgeon, The Erosion Behaviour of NiAl Intermetallic Coatings Produced by High Velocity Oxy-Fuel Thermal Spraying, *Wear*, 1999, **233-235**, p 328-333
20. R.A. Varin, Intermetallics: Crystal Structures, *Encyclopedia of Materials: Science and Technology*, 1st. ed., K.H.J. Buschow, Ed., Elsevier Science Publ. Co., 2001, p 9913, ISBN: 0-08-0431526
21. M. Boufenghour, A. Hayoune, and D. Hamana, Study of the Ordered Structures in Fe-Al Alloys Using Dilatometric and Calorimetric Analysis, *J. Mater. Sci.*, 2004, **39**, p 1207-1212
22. S. Suriñach, X. Amils, S. Gialanella, L. Lutterotti, and M.D. Baro, Kinetics of Reordering in a Nanograined FeAl Alloy, *Mater. Sci. Forum*, 1997, **235-238**, p 415-420
23. http://www.mecachrome.com/
24. D.A. Muller, S. Subramanian, P.E. Batson, J. Silcox, and S.L. Sass, Structure, Chemistry and Bonding at Grain Boundaries in Ni_3Al-I. The Role of Boron in Ductilizing Grain Boundaries, *Acta Mater.*, 1996, **44**(4), p 1637-1645
25. M.M. Rico, J.M. Greneche, and G.A. Perez, Effect of Boron on Structural and Magnetic Properties of the $Fe_{60}Al_{40}$ System Prepared by Mechanical Alloying, *J. Alloys Compd.*, 2005, **398**, p 26-32
26. E. Artz, R. Behr, E. Göhring, P. Grahle, and R.P. Mason, Dispersion Strengthening of Intermetallics, *Mater. Sci. Eng. A*, 1997, **234-236**, p 22-29
27. S. Launois and A. Fraczkiewicz, Environmental Effect on Mechanical Behavior of Reinforced FeAl (40at%Al) Alloy, *J. Phys. IV*, 1996, **6**(2), p C2.223-C2.228
28. G. Ji, T. Grosdidier, N. Bozzolo, and S. Launois, The mechanisms of microstructure formation in a nanostructured oxide dispersion strengthened FeAl alloy obtained by spark plasma sintering, *Intermetallics*, 2007, **15**(2), p 108-118
29. J.M. Guilemany, N. Cinca, C.R.C. Lima, and J.R. Miguel, Studies of Fe40Al Coatings Obtained by High Velocity Oxy-Fuel, *Surf. Coat. Technol.*, 2006, **201**, p 2072-2079
30. J. Xia, C.X. Li, and H. Dong, Thermal Oxidation Treatment of B2 Iron Aluminide for Improved Wear Resistance, *Wear*, 2005, **258**, p 1804-1812
31. J. Gang, J. Morniroli, and T. Grosidider, Nanostructures in Thermal Spray Coatings, *Scr. Mater.*, 2003, **48**, p 1599-1604
32. J.L. Jordan and S.C. Deevi, Vacancy Formation and Effects in FeAl, *Intermetallics*, 2003, **11**, p 507-528
33. H. Skoglund, M. Knutson Wedel, and B. Karlsson, Thermal Vacancy Hardening in Fe(100-x) Alx ($28 < x < 40$), *Intermetallics*, 2007, **15**, p 1127-1131
34. M. Kupka, Can Vacancies be the Main Reason of FeAl Alloys Hardening? *J. Alloys Compd.*, 2007, **437**, p 373-377

35. X. Amils, J. Nogués, S. Suriñach, M.D. Baro, M.A. Muñoz-Morris, and D.G. Morris, Hardening and Softening of FeAl During Milling and Annealing, *Intermetallics*, 2000, **8**, p 805-813
36. K. Holmberg and A. Matthews, *Coatings Tribology Properties, Techniques and Applications in Surface Engineering*, Elsevier Science Publ. Co., Amsterdam, 1994, p 442, ISBN-10: 0444888705 and ISBN-13: 978-0444888709
37. P.J. Alison and H. Wilman, The different behaviour of hexagonal and cubic metals in their friction, wear and work hardening during abrasion, *Brit. J. Appl. Phys.*, 1964, **15**, p 281-289
38. A.Y. Mosbah, D. Wexler, and A. Calka, Abrasive Wear of WC-FeAl Composites, *Wear*, 2005, **258**, p 1337-1341
39. M. Ahmadian, D. Wexler, T. Chandra, and A. Calka, Abrasive Wear of WC-FeAl-B and WC-Ni3AL-B Composites, *Int. J. Refract. Met. Hard Mater.*, 2005, **23**, p 155-159
40. J.M. Guilemany, M. Torrell, and J.R. Miguel, Study of the HVOF Ni-Based Coatings Corrosion Resistance Applied on Municipal Solid-Waste Incinerators, *J. Therm. Spray Technol.*, 2008, **17**(2) p 1059–9630
41. J.M. Guilemany, S. Dosta, and J.R. Miguel, The Enhancement of the Properties of WC-Co HVOF Coatings Through the Use of Nanostructured and Microstructured Feedstock Powders, *Surf. Coat. Technol.*, 2006, **201**, p 1180-1190
42. I.M. Hutchings, *Tribology: Friction and Wear of Engineering Materials*, Metallurgy and Materials Science Series, ISBN 0-340-56184-x
43. Y. Wang, W. Chen, and L. Wang, Micro-Indentation and Erosion Properties of Thermal Sprayed NiAl Intermetallic-Based Alloy Coatings, *Wear*, 2003, **254**, p 350-355
44. B.J. Johnson, F.E. Kennedy, and I. Baker, Dry Sliding Wear of NiAl, *Wear*, 1996, **192**, p 241-247
45. L. Prchlik and S. Sampath, Effect of the Microstructure of Thermally Sprayed Coatings on Friction and Wear Response Under Lubricated and Dry Sliding Conditions, *Wear*, 2007, **262**, p 11-23